Electronic Supplementary Information (ESI)

From Mono- to Tetraacylgermanes: Extending the Scope of Visible Light Photoinitiators

*Anna Eibel,[a] Judith Radebner,[b] Michael Haas,[b] David E. Fast,[a] Hilde Freißmuth,[a] Eduard Stadler,[a] Paul Faschauner,[b] Ana Torvisco,[a] Iris Lamparth[c] Norbert Moszner,[c] Harald Stueger[b] and Georg Gescheidt [a] **

[a] Institute of Physical and Theoretical Chemistry, NAWI Graz, Graz University of Technology, Stremayrgasse 9, 8010 Graz, Austria

[b] Institute of Inorganic Chemistry, NAWI Graz, Graz University of Technology, Stremayrgasse 9, 8010 Graz, Austria

[c] Ivoclar Vivadent AG, Bendererstrasse 2, 9494 Schaan, Liechtenstein

1. UV-Vis

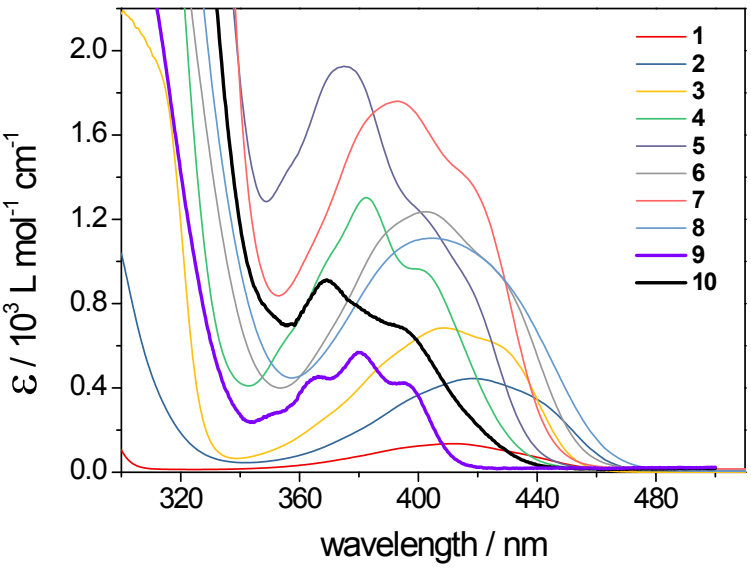

Figure S1. UV-Vis spectra of mono- and bisacylphosphane oxides **9** and **10** (bold lines) and comparison to UV-Vis spectra of acylgermanes **1**-**8**, recorded in acetonitrile.

2. Photobleaching

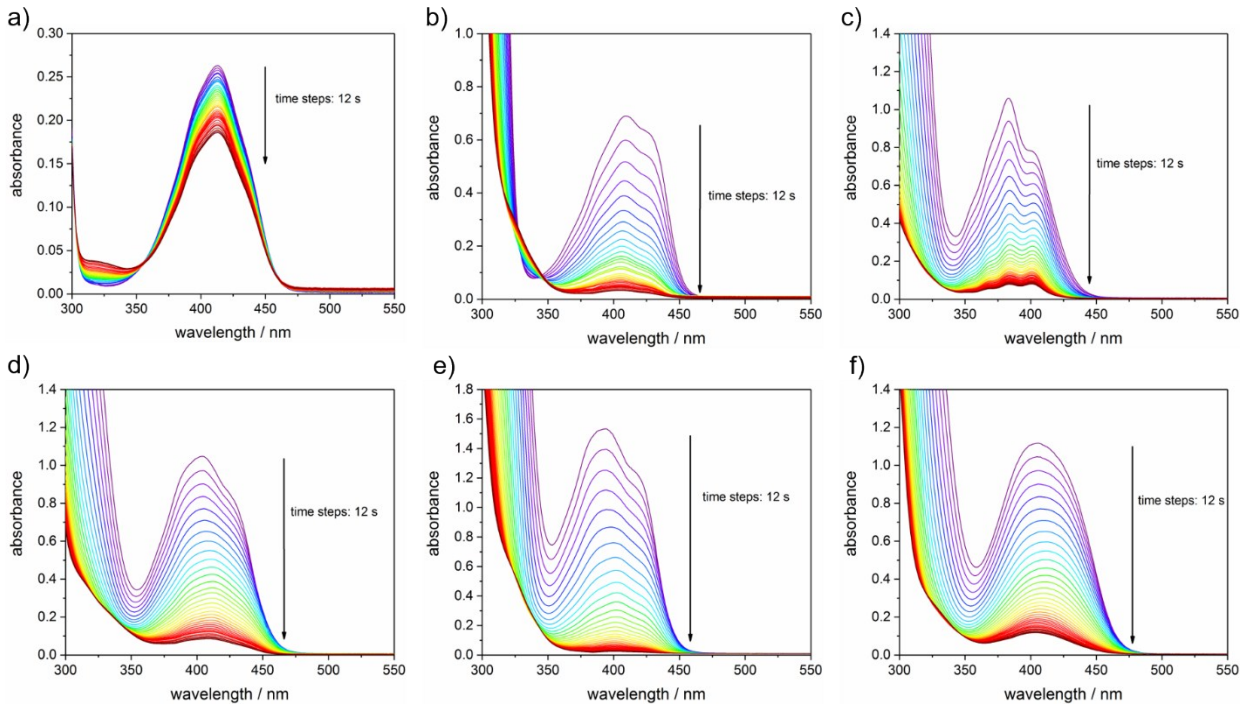

Figure S2. UV-vis spectra recorded upon irradiation at 385 nm (LED385) of compounds: a) **1** (*c* = 2 mM) b) **3** (*c* = 1 mM), c) **4** (*c* = 0.8 mM), d) **6** (*c* = 0.8 mM), e) **7** (*c* = 0.8 mM), f) **8** (*c* = 0.8 mM). Samples were prepared in acetonitrile/MMA (1/1 v/v) and were saturated with argon before the measurement.

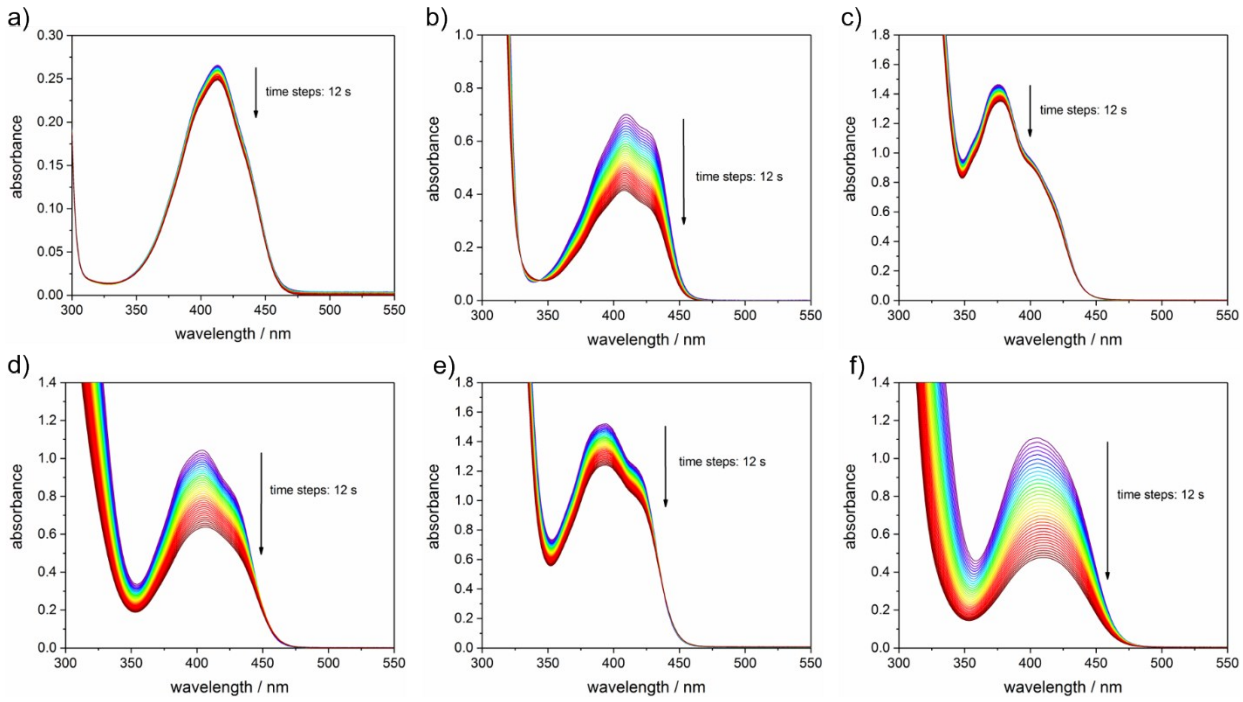

Figure S3. UV-vis spectra recorded upon irradiation at 470 nm (LED470) of compounds: a) **1** (*c* = 2 mM) b) **3** (*c* = 1 mM), c) **4** (*c* = 0.8 mM), d) **6** (*c* = 0.8 mM), e) **7** (*c* = 0.8 mM), f) **8** (*c* = 0.8 mM). Samples were prepared in acetonitrile/MMA (1/1 v/v) and were saturated with argon before the measurement.

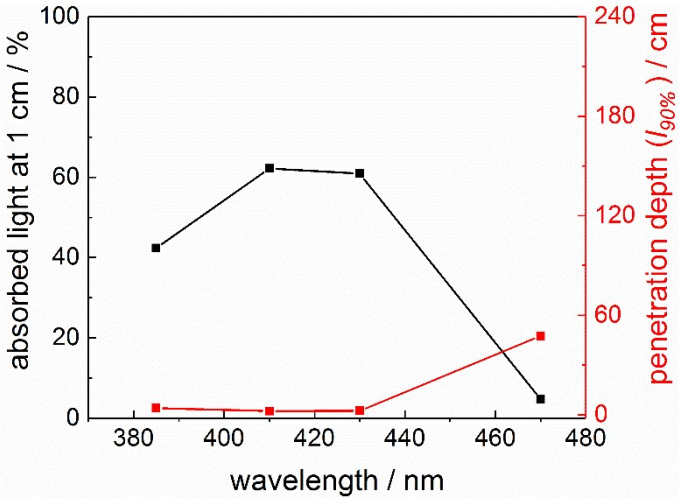

Figure S4. Plots of absorbed light at a path length *l* of 1 cm and calculated penetration depth $I_{90\%}$ for a 1 mM solution of compound **2**. Lines are to guide the eye.

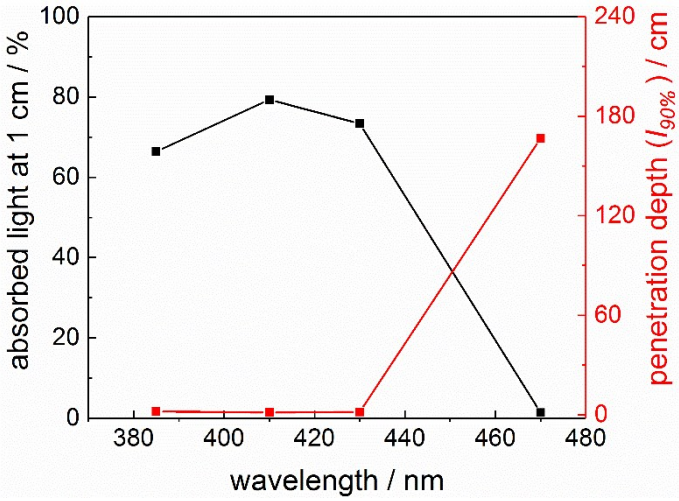

Figure S5. Plots of absorbed light at a path length *l* of 1 cm and calculated penetration depth $I_{90\%}$ for a 1 mM solution of compound **3**. Lines are to guide the eye.

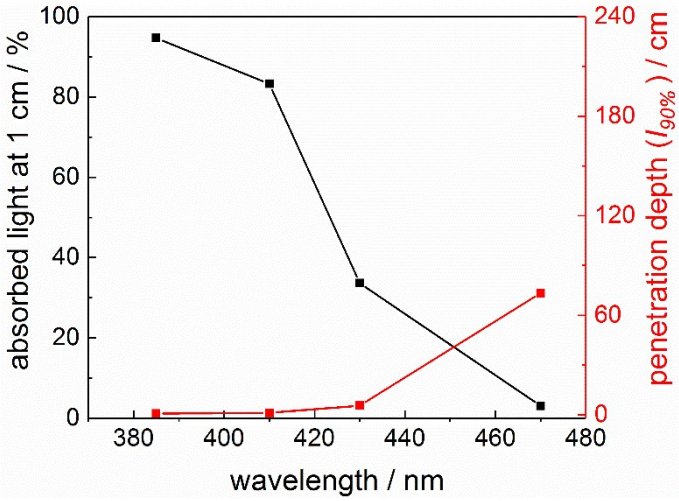

Figure S6. Plots of absorbed light at a path length *l* of 1 cm and calculated penetration depth $I_{90\%}$ for a 1 mM solution of compound **4**. Lines are to guide the eye.

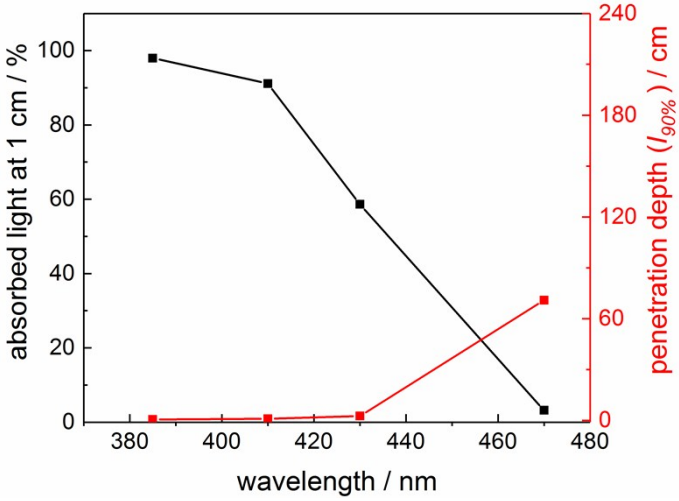

Figure S7. Plots of absorbed light at a path length *l* of 1 cm and calculated penetration depth $I_{90\%}$ for a 1 mM solution of compound **5**. Lines are to guide the eye.

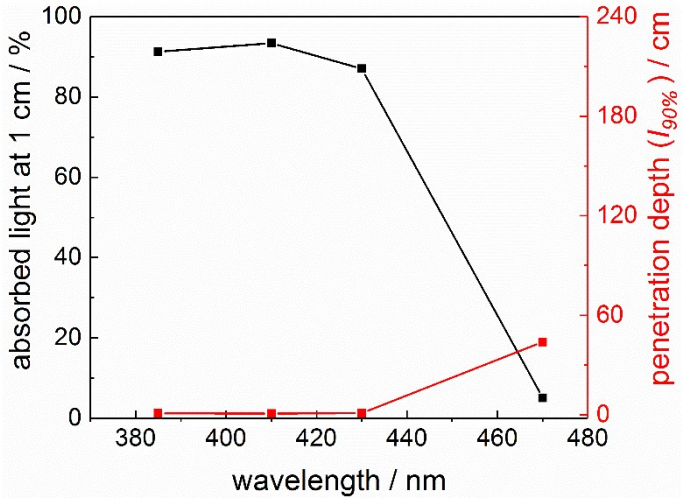

Figure S8. Plots of absorbed light at a path length *l* of 1 cm and calculated penetration depth $l_{90\%}$ for a 1 mM solution of compound **6**. Lines are to guide the eye.

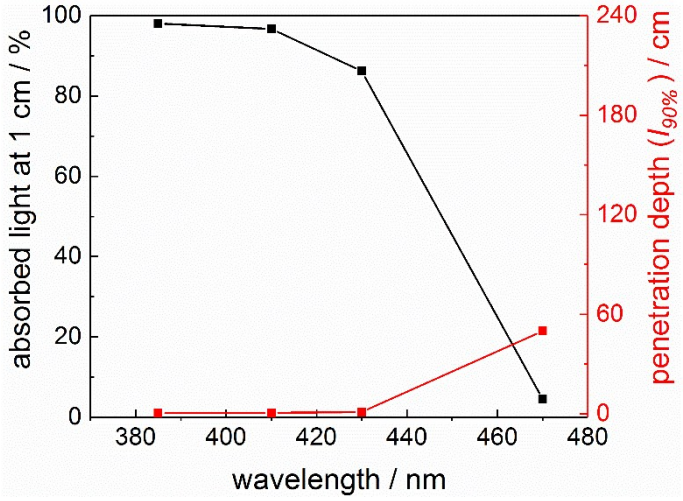

Figure S9. Plots of absorbed light at a path length *l* of 1 cm and calculated penetration depth $l_{90\%}$ for a 1 mM solution of compound **7**. Lines are to guide the eye.

Table S1. Summary of experimental extinction coefficients (ε, determined in acetonitrile) and calculated values for absorbed light at 1 cm (A_{1cm}) and penetration depth ($l_{90\%}$) for 1 mM solutions. Error bars for ε values have been determined from four individual measurements.

Compound	Wavelength / nm	ε/ L mol^{-1} cm^{-1}	A_{1cm}	$l_{90\%}$
1	470	4.5 ± 0.7	1.0	222.2
	430	99.9 ± 2.0	20.5	10.0
	410	135.0 ± 3.0	26.7	7.4
	385	89.6 ± 1.8	18.6	11.2
2	470	21.0 ± 1.9	4.7	47.5
	430	407.9 ± 6.3	60.9	2.5
	410	422.2 ± 6.1	62.2	2.4
	385	239.2 ± 5.0	42.3	4.2
3	470	6.0 ± 3.9	1.4	166.7
	430	574.5 ± 3.6	73.4	1.7
	410	683.3 ± 4.8	79.3	1.5
	385	473.8 ± 2.6	66.4	2.1
4	470	13.6 ± 1.1	3.1	73.4
	430	178.1 ± 1.6	33.6	5.6
	410	776.4 ± 9.6	83.3	1.3
	385	1271.9 ± 18.5	94.7	0.8
5	470	14.1 ± 6.0	3.2	70.9
	430	383.1 ± 7.5	58.6	2.6
	410	1052.4 ± 11.5	91.1	1.0
	385	1694.2 ± 16.5	98.0	0.6
6	470	22.7 ± 3.9	5.1	44.0
	430	885.7 ± 7.9	87.0	1.1
	410	1181.0 ± 15.1	93.4	0.8
	385	1057.1 ± 10.5	91.2	0.9
7	470	20.0 ± 6.5	4.5	49.9
	430	858.1 ± 7.7	86.1	1.2
	410	1479.0 ± 7.7	96.7	0.7
	385	1707.0 ± 24.3	98.0	0.6
8	470	48.8 ± 1.0	10.6	20.5
	430	894.7 ± 15.0	87.3	1.1
	410	1100.0 ± 17.2	92.1	0.9
	385	929.2 ± 9.4	88.2	1.1

3. Quantum Yields of Decomposition

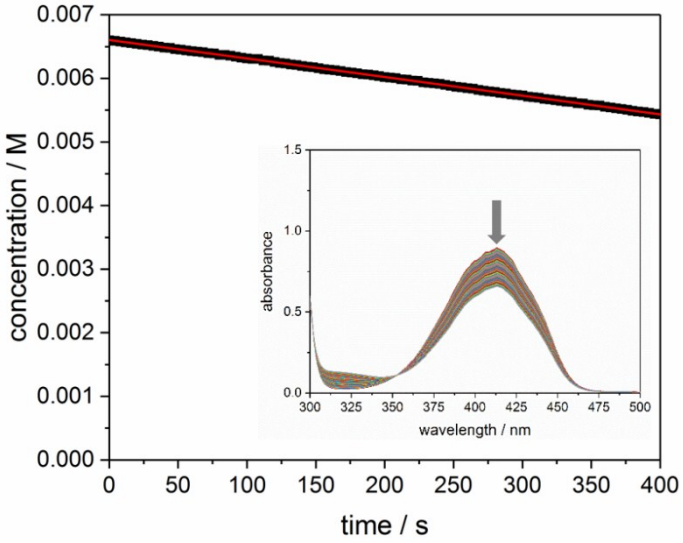

Figure S10. Decay of concentration vs. irradiation time for compound **1**, monitored at 413.0 nm, together with the exponential fit (red line). The inset shows the corresponding UV-Vis spectra (time steps between each spectrum: 12 s, sample: 7 mM **1** in acetonitrile/MMA (1/1 v/v).)

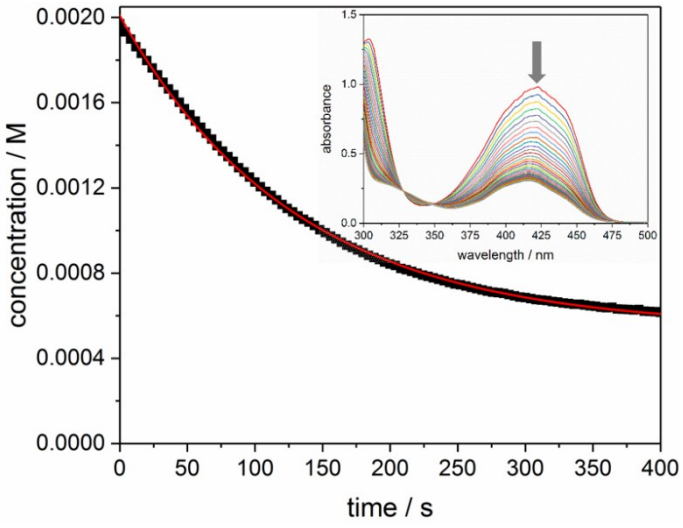

Figure S11. Decay of concentration vs. irradiation time for compound **2**, monitored at 420.0 nm, together with the exponential fit (red line). The inset shows the corresponding UV-Vis spectra (time steps between each spectrum: 12 s, sample: 2 mM **2** in acetonitrile/MMA (1/1 v/v).)

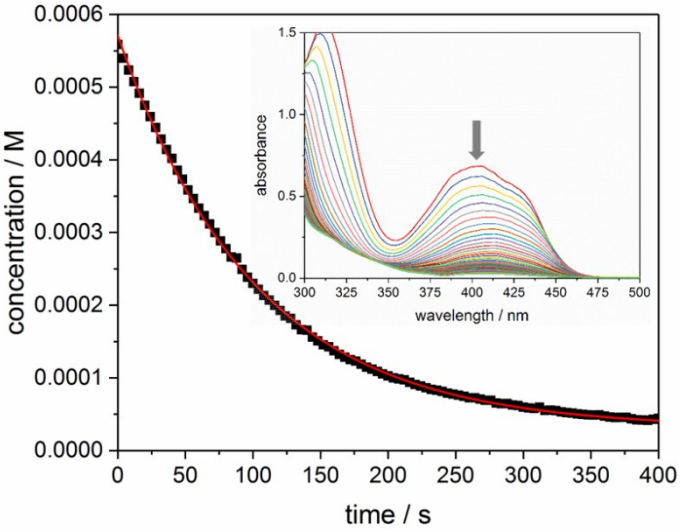

Figure S12. Decay of concentration vs. irradiation time for compound **6**, monitored at 403.5 nm, together with the exponential fit (red line). The inset shows the corresponding UV-Vis spectra (time steps between each spectrum: 12 s, sample: 0.6 mM **6** in acetonitrile/MMA (1/1 v/v).)

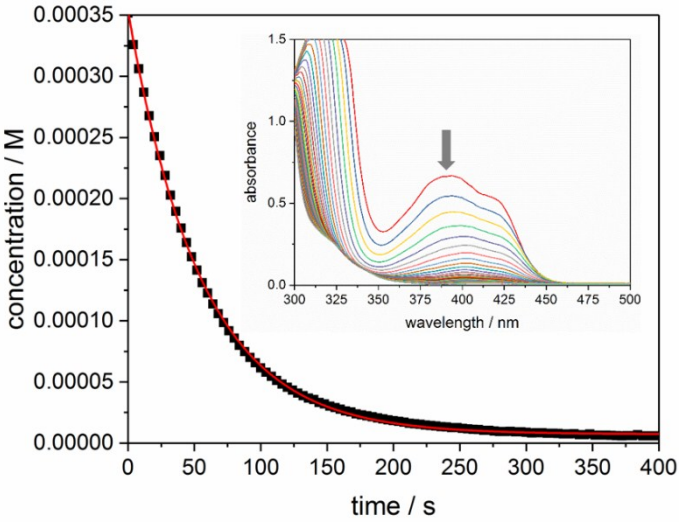

Figure S13. Decay of concentration vs. irradiation time for compound **7**, monitored at 394 nm, together with the exponential fit (red line). The inset shows the corresponding UV-Vis spectra (time steps between each spectrum: 12 s, sample: 0.35 mM **7** in acetonitrile/MMA (1/1 v/v).)

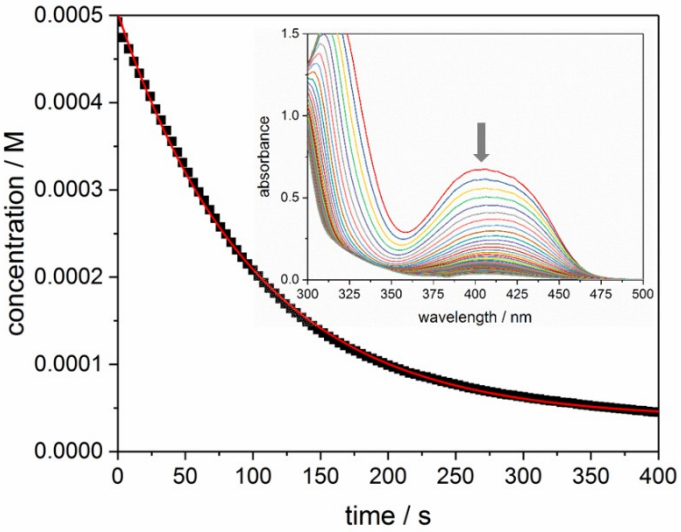

Figure S14. Decay of concentration vs. irradiation time for compound **8**, monitored at 405.5 nm, together with the exponential fit (red line). The inset shows the corresponding UV-Vis spectra (time steps between each spectrum: 12 s, sample: 0.5 mM **8** in acetonitrile/MMA (1/1 v/v).)

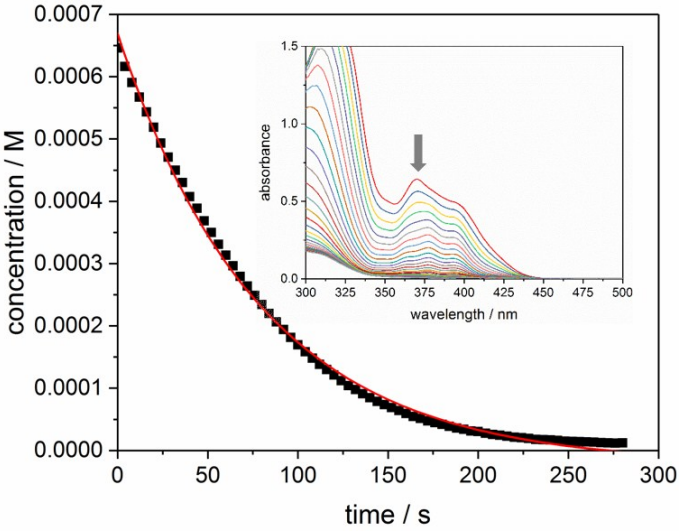

Figure S15. Decay of concentration vs. irradiation time for compound **10**, monitored at 370 nm, together with the exponential fit (red line). The inset shows the corresponding UV-Vis spectra (time steps between each spectrum: 12 s, sample: 0.7 mM **10** in acetonitrile/MMA (1/1 v/v).)

4. Laser-flash Photolysis

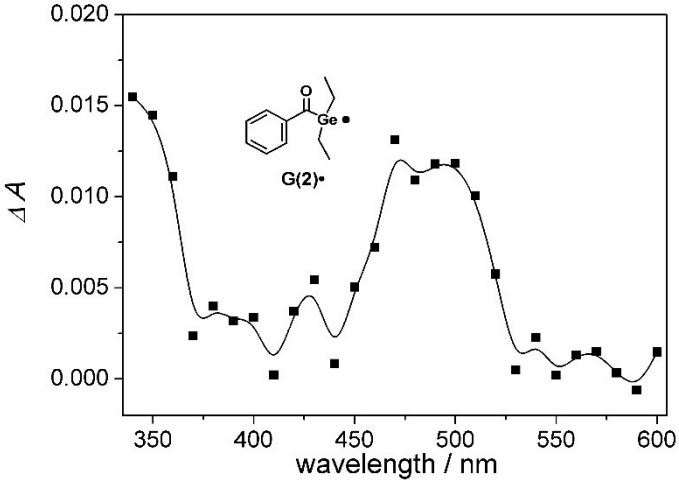

Figure S16. Transient optical absorption spectrum (absorbance change *ΔA* versus wavelength) of radical **G(2)•** recorded 200 – 300 ns after laser excitation (355 nm, 8 ns) of **2** in argon-saturated acetonitrile solutions (A_{355} ~ 0.3).

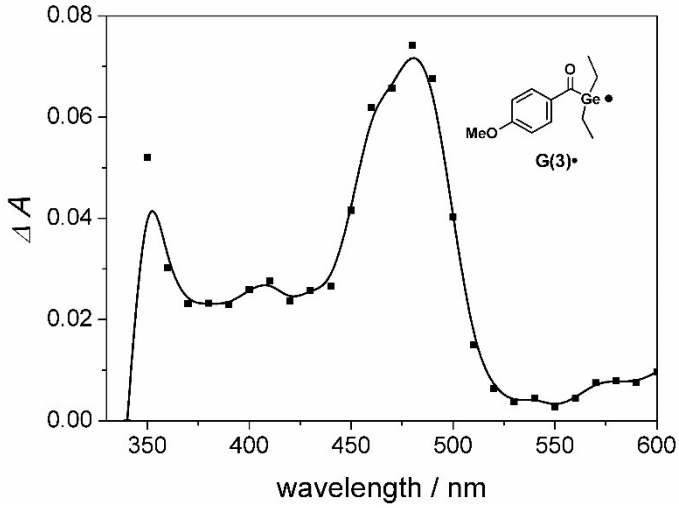

Figure S17. Transient optical absorption spectrum (absorbance change *ΔA* versus wavelength) of radical **G(3)•** recorded 200 – 300 ns after laser excitation (355 nm, 8 ns) of **3** in argon-saturated acetonitrile solutions (A_{355} ~ 0.3).

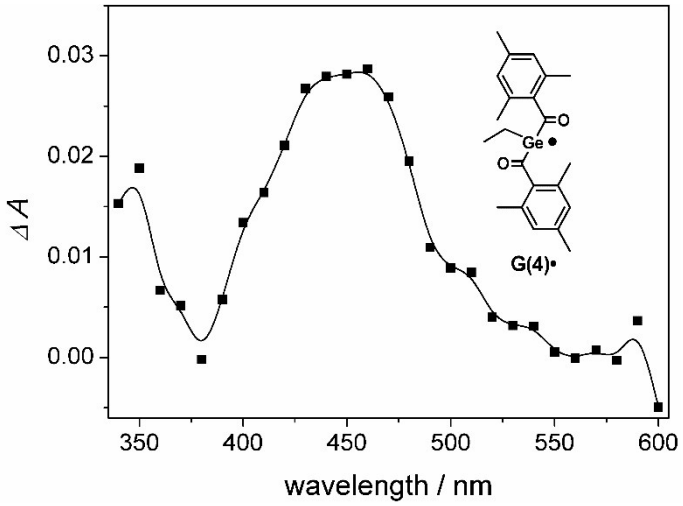

Figure S18. Transient optical absorption spectrum (absorbance change *ΔA* versus wavelength) of radical **G(4)•** recorded 200 – 300 ns after laser excitation (355 nm, 8 ns) of **4** in argon-saturated acetonitrile solutions (A_{355} ~ 0.3).

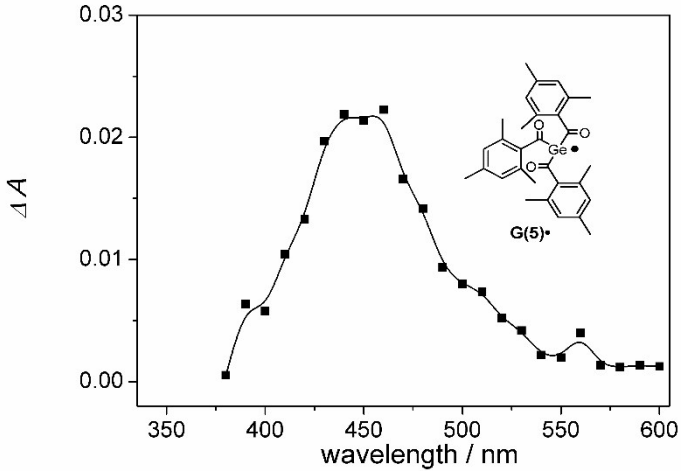

Figure S19. Transient optical absorption spectrum (absorbance change *ΔA* versus wavelength) of radical **G(5)•** recorded 200 – 300 ns after laser excitation (355 nm, 8 ns) of **5** in argon-saturated acetonitrile solutions (A_{355} ~ 0.3).

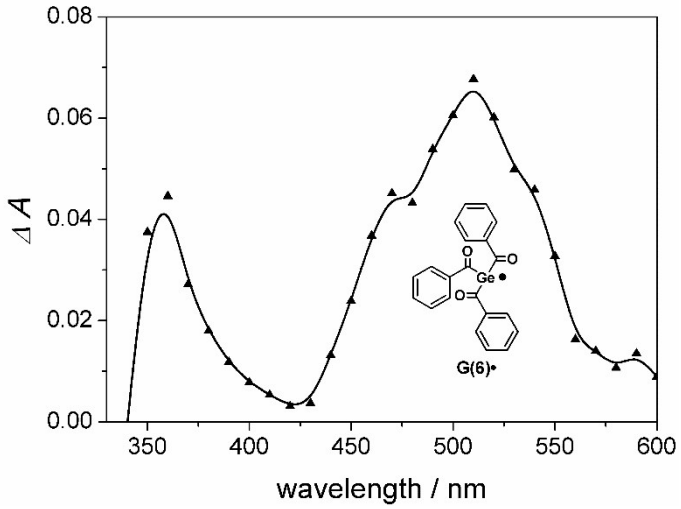

Figure S20. Transient optical absorption spectrum (absorbance change *ΔA* versus wavelength) of radical **G(6)•** recorded 200 – 300 ns after laser excitation (355 nm, 8 ns) of **6** in argon-saturated acetonitrile solutions (A_{355} ~ 0.3).

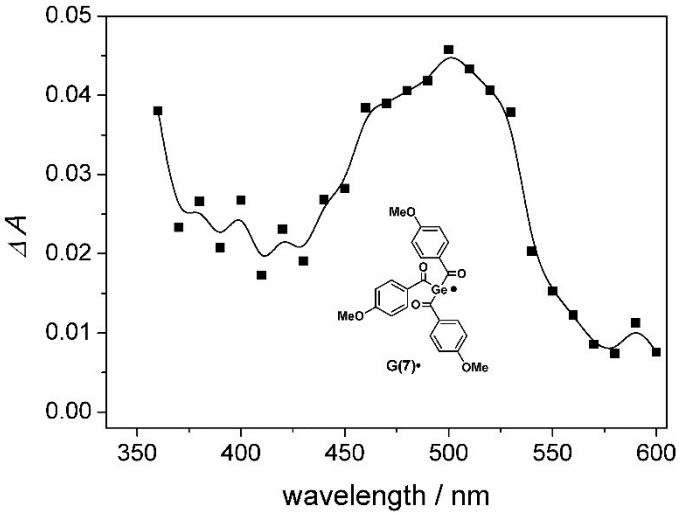

Figure S21. Transient optical absorption spectrum (absorbance change *ΔA* versus wavelength) of radical **G(7)•** recorded 200 – 300 ns after laser excitation (355 nm, 8 ns) of **7** in argon-saturated acetonitrile solutions (A_{355} ~ 0.3).

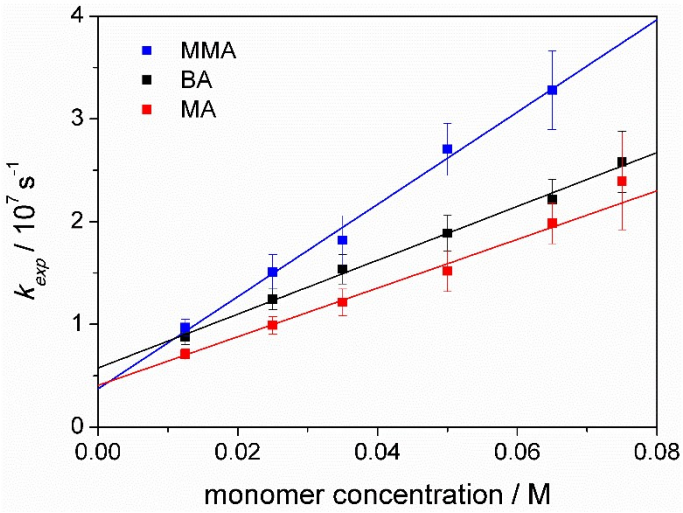

Figure S22. Pseudo-first-order decay rate constant (k_{exp}) of radical **G(2)•** versus monomer concentration; laser flash photolysis of argon-saturated acetonitrile solutions of **2** in the presence of monomers (excitation wavelength: 355 nm, monitoring wavelength: 500 nm).

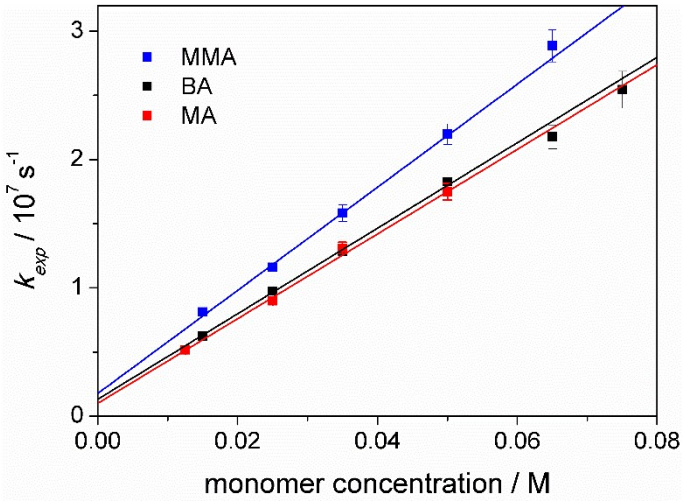

Figure S23. Pseudo-first-order decay rate constant (k_{exp}) of radical **G(3)•** versus monomer concentration; laser flash photolysis of argon-saturated acetonitrile solutions of **3** in the presence of monomers (excitation wavelength: 355 nm, monitoring wavelength: 480 nm).

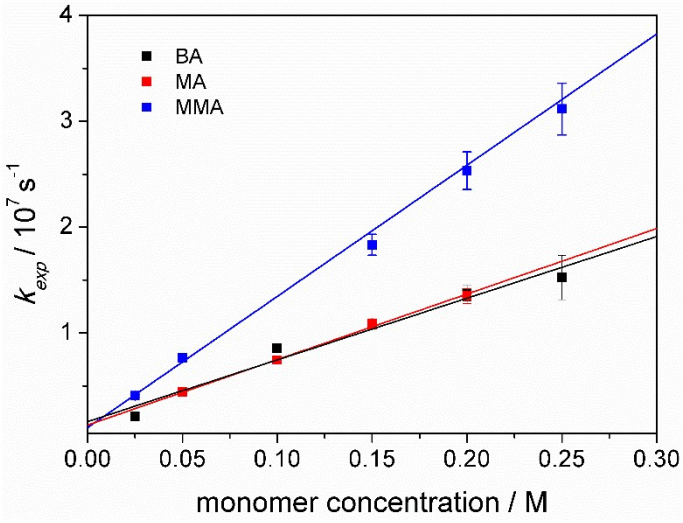

Figure S24. Pseudo-first-order decay rate constant (k_{exp}) of radical **G(4)•** versus monomer concentration; laser flash photolysis of argon-saturated acetonitrile solutions of **4** in the presence of monomers (excitation wavelength: 355 nm, monitoring wavelength: 470 nm).

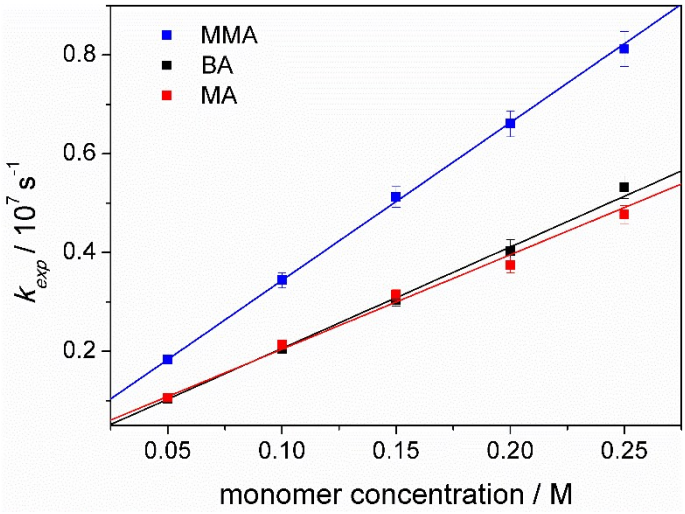

Figure S25. Pseudo-first-order decay rate constant (k_{exp}) of radical **G(5)•** versus monomer concentration; laser flash photolysis of argon-saturated acetonitrile solutions of **5** in the presence of monomers (excitation wavelength: 355 nm, monitoring wavelength: 450 nm).

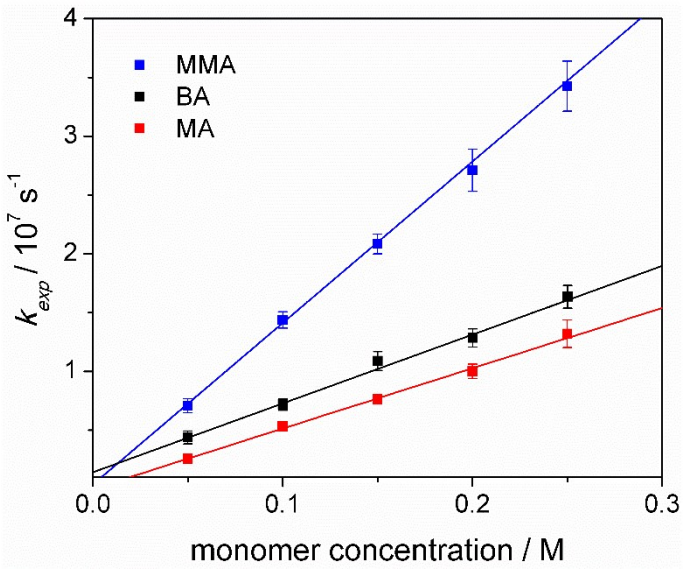

Figure S26. Pseudo-first-order decay rate constant (k_{exp}) of radical **G(6)•** versus monomer concentration; laser flash photolysis of argon-saturated acetonitrile solutions of **6** in the presence of monomers (excitation wavelength: 355 nm, monitoring wavelength: 510 nm).

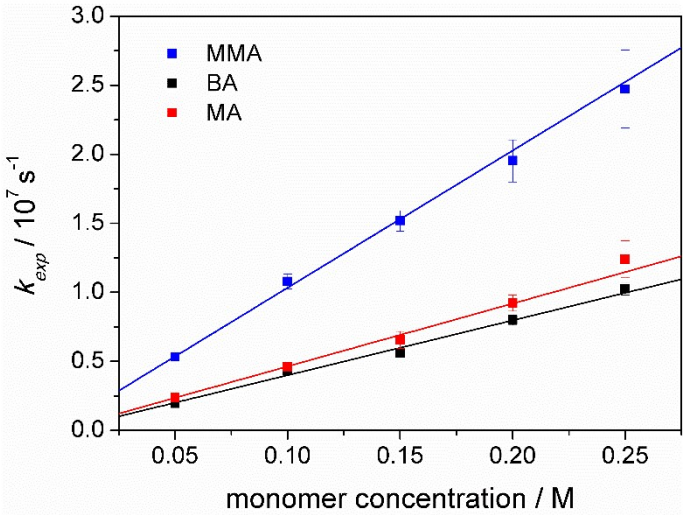

Figure S27. Pseudo-first-order decay rate constant (k_{exp}) of radical **G(7)•** versus monomer concentration; laser flash photolysis of argon-saturated acetonitrile solutions of **7** in the presence of monomers (excitation wavelength: 355 nm, monitoring wavelength: 490 nm).

5. CIDNP Spectroscopy

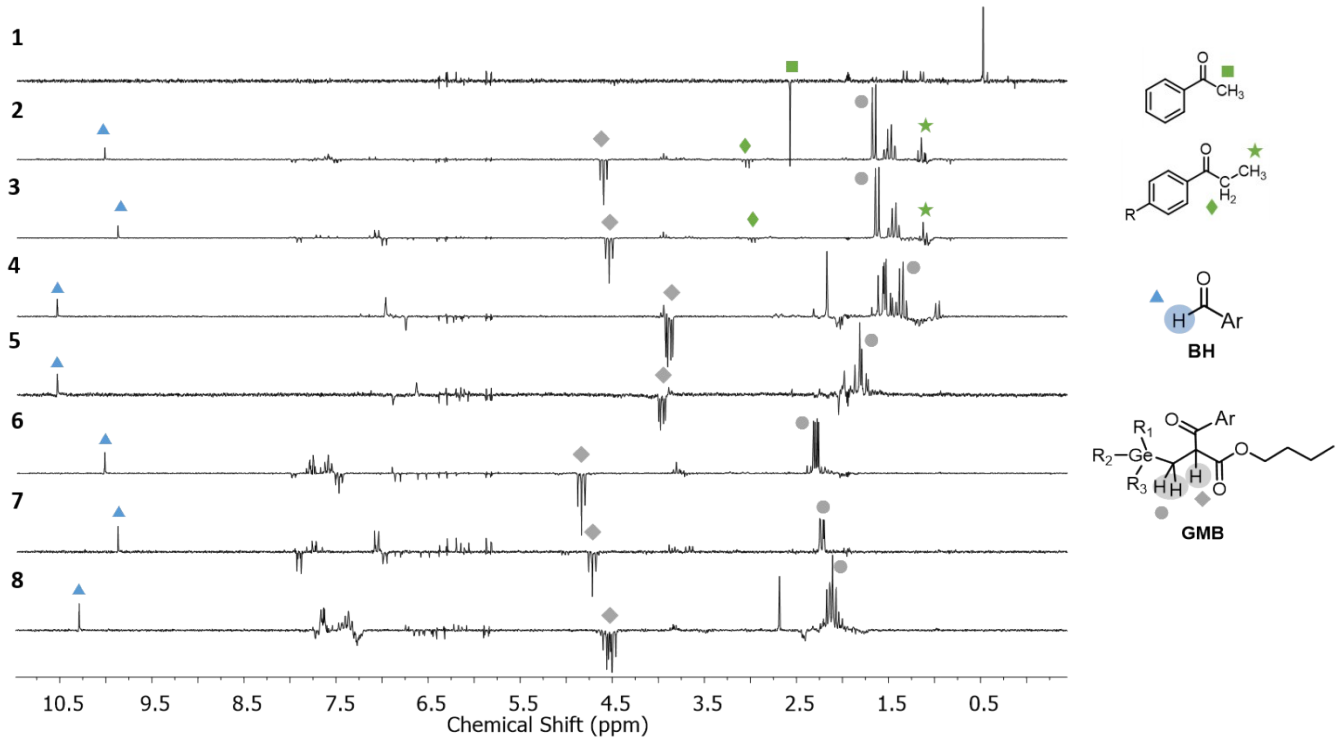

Figure S28. ^{1}H CIDNP spectra (excitation at λ = 355 nm, *ca.* 70 mJ/pulse) of compounds **1**–**8** recorded in acetonitrile-d_3 in the presence of butyl acrylate together with the assigned products. Compound **1** does not show the radical-to-monomer addition product **GMB** and the aldehyde **BH**.

6. X-ray Crystallography

A crystal suitable for single crystal X-ray diffractometry was removed from a vial and immediately covered with a layer of silicone oil. A single crystal was selected, mounted on a glass rod on a copper pin, and placed in the cold N_2 stream provided by an Oxford Cryosystems cryostream. XRD data collection was performed on a Bruker APEX II diffractometer with use of an Incoatec microfocus sealed tube of Mo Kα radiation (λ = 0.71073 Å) and a CCD area detector. Empirical absorption corrections were applied using SADABS or TWINABS.[1-2] The structure was solved with use of the intrinsic phasing option in SHELXT and refined by the full-matrix least-squares procedures in SHELXL.[3-5] The space group assignment and structural solution were evaluated using PLATON.[6-7] Non-hydrogen atoms were refined anisotropically. Hydrogen atoms were located in calculated positions corresponding to standard bond lengths and angles. Compound $Ge(C{=}OMes)_3Et$ (**4**) was twinned and was refined using the TWIN option in SHELXL and the matrix (-1 0 0 0 -1 0 0 0 -1) was applied. The main contributions of the two twin components refined to a BASF of 0.06. CCDC 1561720 contains the supplementary crystallographic data for the compound. This data can be obtained free of charge from The Cambridge Crystallographic Data Centre via www.ccdc.cam.ac.uk/data_request/cif. Table S2 contains crystallographic data and details of measurements and refinement for compound **4**.

Table S2. Crystallographic data and details of measurements for compound **4**.

Mo Kα (λ=0.71073Å). R1 = Σ/ $|F_o|$- $|F_c|$/$|\Sigma|F_d$; wR2 = $[\Sigma_w(F_o^2-F_2^2)^2/ \Sigma_w(F_o^2)^2]^{1/2}$

Compound	**4**
Formula	$C_{32}H_{38}GeO_3$
Fw (g mol^{-1})	543.21
a (Å)	14.4530(6)
b (Å)	24.1484(10)
c (Å)	24.504(10)
α (°)	90
β (°)	90
γ (°)	90
V ($Å^3$)	8552.3(6)
Z	12
Crystal size (mm)	0.15 × 0.10 × 0.09
Crystal habit	Block, colourless
Crystal system	Orthorhombic
Space group	$P2_12_12_1$
d_{calc} (mg/m^3)	1.266
μ (mm^{-1})	1.104
T (K)	100(2)
2ϑ range (°)	2.2–30.0
F(000)	3432
R_{int}	0.088
independent reflns	32647
No. of params	1003
R1, wR2 (all data)	R1 = 0.0629 wR2 = 0.1051
R1, wR2 (>2σ)	R1 = 0.0443 wR2 = 0.0962

References

1. Bruker *APEX2 and SAINT*, Bruker AXS Inc.: Madison, Wisconsin, USA, 2012.

2. Blessing, R., An empirical correction for absorption anisotropy. *Acta Crystallogr., Sect. A* **1995,** *51* (1), 33-38.

3. Sheldrick, G., Phase annealing in SHELX-90: direct methods for larger structures. *Acta Crystallogr., Sect. A* **1990,** *46* (6), 467-473.

4. Sheldrick, G., A short history of SHELX. *Acta Crystallogr., Sect. A* **2008,** *64* (1), 112-122.

5. Sheldrick, G. M., SHELXT - Integrated space-group and crystal-structure determination. *Acta Crystallogr., Sect. A: Found. Adv.* **2015,** *71* (1), 3-8.

6. Spek, A. L., Single-crystal structure validation with the program PLATON. *Journal of Applied Crystallography* **2003,** *36* (1), 7-13.

7. Spek, A. L., Structure validation in chemical crystallography. *Acta Crystallographica Section D* **2009,** *65* (2).